

# Dynamics and noise of fiber-grating semiconductor lasers affected by the line-width enhancement factor

Salah ABDULRHMAN

*Department of Physics, Faculty of Science, Jazan University, Jazan-KSA*  
*Department of Physics, Faculty of Science, Assiut University, Assiut-EGYPT*  
*e-mail: abdulrhmanns@yahoo.com*

Received: 09.05.2011

## Abstract

This paper numerically investigates the effect of the line-width enhancement factor on the dynamics and the intensity noise of InGaAs/InP lasers pumping in the wavelength of 980 nm at the strong optical feedback limit. The investigation is performed based on an improved time-delay rate equation model of a single-mode laser. The analyses are performed in terms of the temporal trajectory of the laser intensity, bifurcation diagram, relative intensity noise and injection current. The simulation results indicate that the laser, under strong optical feedback, mainly operates in CW, pulsation or chaos operation depending on the line-width enhancement factor and injection current values. At larger values of the line-width enhancement factor and injection current the pulsing operation becomes more dominant over wider range of strong optical feedback. The corresponding relative intensity noise level is close to or slightly larger than the level of the solitary laser noise. The optical feedback noise is found to be as low as the quantum noise level when the laser is operated in pulsing region and at larger values of the line-width enhancement factor and injection current.

**Key Words:** Semiconductor laser, strong optical feedback, intensity noise

## 1. Introduction

Semiconductor lasers (SLs) are known to be extremely sensitive to the optical feedback (OFB) occurring when a portion of the laser output is fed back into the laser cavity after being reflected from an external reflecting surface. The effect of OFB on SLs has been extensively studied in references [1–4].

Recently InGaAs lasers emitting in the wavelength of 980 nm have received much interest as pumping sources for fiber amplifiers in fiber communication systems. In such systems, an external cavity is formed between the laser front facet and a fiber grating (FG). The pumping lasers are designed with a low front-facet reflectivity compared with that of the gratings and are then subjected to strong OFB [5]. Moreover, the laser operation is influenced by intrinsic fluctuations in the intensity and optical phase of the lasing field due to transition of electrons between the conduction and valence bands [6], which may modulate the influence of the OFB on the laser dynamics. Most previous models of OFB were applicable under weak or moderate

OFB and were based on a small-signal approximation [4, 7, 8], which overlooks time variations of the lasing parameters. In [8–13], the first author took part in developing a versatile time delay model to analyze operation of semiconductor lasers under an arbitrary amount of OFB.

Furthermore, the line-width enhancement factor, also known as  $\alpha$ -factor, has a great importance for SLs, as it is one of the main features that distinguish the behavior of SLs with respect to other types of lasers. The  $\alpha$ -factor influences several fundamental aspects of SLs, such as the line-width, the chirp under current modulation, the mode stability, the occurrence of filamentation in broad-area devices [14]. Theoretical studies on the effect of the  $\alpha$ -factor on the operation and noise of SLs subject to OFB show that SLs dynamics are strongly dependent on the value of the  $\alpha$ -factor [15–21]. Therefore, knowledge and understanding of the effect of the  $\alpha$ -factor on the SLs dynamics under strong OFB is indispensable to stabilize the device emission and optimize its design and operating conditions.

In this article, we apply the time-delay model in [9] to run intensive computer simulations of 980 nm InGaAs/InP FGSLs with a long fiber cavity using a wide range of the  $\alpha$ -factor. The study is based on the bifurcation diagram analysis of the temporal trajectory of the laser intensity over wide range of the OFB strength and injection current. The laser dynamics under strong OFB are simulated by numerical integration of the modified rate equations presented in reference [9], which are superposed by Langevin noise sources to include the influence of the intrinsic fluctuations.

## 2. Theoretical model of simulation

We apply the model in [9] to investigate the effect of the  $\alpha$ -factor on noise and operation dynamics of FGSLs. In [9], it was shown that counting a single roundtrip is enough to describe the OFB phenomenon in the case of a long external cavity. We reduce the model in our paper [9] to the limit of a single roundtrip. The external power reflectivity  $R_{ex}$ , refractive index  $n_{ex}$  and length of external cavity  $L_{ex}$  are changed to  $R_g$  of the grating and  $n_F$  and  $L_F$  of the fiber cavity, respectively, as shown in Figure 1. The time-delay rate equations describing the FGSL dynamics are described by the following system of equations:

$$\frac{dS}{dt} = \left\{ \frac{a\xi}{V}(N - N_g) - BS - G_{th0} + \frac{c}{n_D L_D} \ln|T| \right\} S + \frac{a\xi}{V} N + F_S(t), \quad (1)$$

$$\frac{d\theta}{dt} = \frac{\alpha a \xi}{2V}(N - \bar{N}) - \frac{c}{2n_D L_D}(\phi - \bar{\phi}) + F_\theta(t), \quad (2)$$

$$\frac{dN}{dt} = -\frac{a\xi}{V}(N - N_g)S - \frac{N}{\tau_s} + \frac{I}{e} + F_N(t), \quad (3)$$

where  $a\xi(N - N_g)/V$  is the linear gain coefficient with  $a$  and  $N_g$  as material constants and  $\xi$  as the confinement factor of the optical field into the active region of volume  $V$ .  $\alpha$  is the line-width enhancement factor, and  $I$  is the injection current. The coefficient  $B$  describes the nonlinear suppression of gain, and is given by [22, 23]

$$B = \frac{9\hbar\omega_o}{4\varepsilon_o n_D^2} \left( \frac{\tau_{in}}{\hbar} \right)^2 \left( \frac{\xi}{V} \right)^2 a |R_{cv}|^2 (N - N_s),$$

$$B = B_c (N - N_s), \quad (4)$$

where  $R_{cv}$  is the dipole moment,  $\tau_{in}$  is the intra-band relaxation time,  $N_s$  is an injection level characterizing the nonlinear gain and  $B_c$  is the nonlinear gain coefficient.

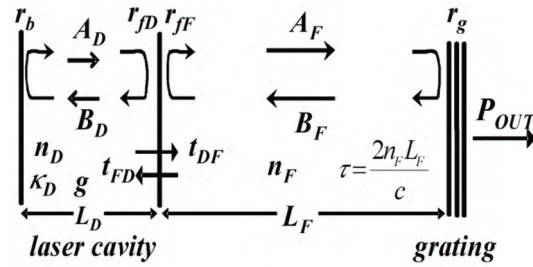


**Figure 1.** Schematic illustration of a time-delay model of SLs under OFB [9].

The complex coefficient  $T$  describes the influence of OFB on the threshold conditions is given by [9]

$$T = 1 - (1 - R_f) \sqrt{\frac{R_g}{R_f}} e^{-j\psi} \sqrt{\frac{S(t-\tau)}{S(t)}} \frac{e^{j\theta(t-\tau)}}{e^{j\theta(t)}} = |T| e^{-j\phi}. \quad (5)$$

Here,  $\psi$  is the phase difference between delayed light in the external cavity and the reflected field at the front facet of the laser cavity,  $\omega$  is the emission circular frequency and  $\tau = 2\pi n_F L_F / c$  is the roundtrip time.

The functions  $F_S(t)$ ,  $F_N(t)$  and  $F_\theta(t)$  are the Langevin noise sources and are assumed to have Gaussian probability distributions with their correlation functions defined as

$$\langle F_x(t) F_y(t') \rangle = V_{xy} \delta(t - t'), \quad x, y = S, N \text{ or } \theta, \quad (6)$$

where  $\delta(t - t')$  is Dirac's  $\delta$  function and the quantities  $V_{xy}$  are the variances of the correlations and are determined by the mean values of  $S$  and  $N$  at each electron transition process of equations (1)–(3). It should be noted that the noise sources  $F_S(t)$  and  $F_\theta(t)$  are uncorrelated, i.e.,  $V_{S\theta} = 0$ . It is the necessity that the noise sources satisfy the above conditions of auto and cross-correlations. The procedures of generating the noise sources are described in [8].

The corresponding output power from back facet  $P_b(t)$  and output power from the FG,  $P_g(t)$ , of the photon number inside the laser cavity  $S(t)$  as well as in the external photon number, respectively are determined from the following relations [8]:

$$P_b = [\hbar\omega c / (2n_D L_D)] |T| S (1 - R_b) \sqrt{R_f / R_b} \times \left\{ \frac{[1/2 \ln(1/R_f R_b) + \ln 1/|T|]}{[1 + (1/\sqrt{R_b} - \sqrt{R_b}) \sqrt{R_f} |T| - |T|^2 R_f]} \right\}, \quad (7)$$

$$P_g = [\hbar\omega c / (2n_F L_D)] (n_F / n_D) |U|^2 S (1 - R_g) (1 - R_f) \times \left\{ \frac{[1/2 \ln(1/R_f R_b) + \ln 1/|T|]}{[1 + (1/\sqrt{R_b} - \sqrt{R_b}) \sqrt{R_f} |T| - |T|^2 R_f]} \right\}. \quad (8)$$

Here, the transmission function  $U$  is given by

$$U = 1 + (R_g R_f)^{1/2} e^{-jm\psi} \sqrt{\frac{S(t-\tau)}{S(t)}} e^{j(\theta(t-\tau) - \theta(t))}. \quad (9)$$

### 3. Numerical calculations

We numerically integrated the time-delay rate equations (1)–(3) via the fourth-order Runge-Kutta method using a time interval of 5 ps over a long period of 10  $\mu$ s. The relative intensity noise (RIN) was calculated as the power density function of the fluctuations in the output power  $\delta P(t) = P(t) - \bar{P}$  divided by  $\bar{P}^2$ , where  $\bar{P}$  is the DC value of  $P(t)$ . The calculations of RIN were carried out when the operation becomes stable ( $t \approx 8 \sim 10$   $\mu$ s). The applied numerical values of InGaAs/Inp lasers are given in Table 1.

**Table 1.** List of the parameters of 980 nm InGaAs/InP lasers and their typical values used in the calculations.

Parameter	Value	Units
Refractive index of external cavity $n_F$	1.5	—
Tangential coefficient of gain $a$	$2.21 \times 10^{-12}$	$\text{m}^3\text{s}^{-1}$
Electron number at transparency $N_g$	$4.08 \times 10^8$	—
Nonlinear gain coefficient $B_c$	$2.2 \times 10^{-6}$	$\text{s}^{-1}$
Electron number characterizing $B, N_s$	$1.53 \times 10^8$	—
Electron life time $\tau_s$	2.79	ns
Refractive index of active region $n_D$	3.5	—
Length of the active region $L_D$	800	$\mu\text{m}$
Length of the external cavity $L_F$	80	cm
Volume of the active region $V$	400	$\mu\text{m}^3$
Field confinement factor $\xi$	0.1	—
Reflectivity at front facet $R_f$	0.02	—
Reflectivity at back facet $R_b$	0.98	—

### 4. Simulation results and discussions

#### 4.1. Bifurcation diagrams and relative intensity noise

In order to understand the behavior of the FGSL under strong OFB, we simulate the laser dynamics over a wide range of  $\alpha$ -factors and ratios  $R_g/R_f$ . Value of semiconductor laser  $\alpha$ -factor depends on laser design and injection current; and, conversely, any increase in the injection current may, in general, lead to rapid or dramatic increases in the  $\alpha$ -factor [15, 24, and 25]. Thus in the present work,  $\alpha$ -factor is changed between zero and 6.

Simulation is performed by means of a bifurcation diagram of the output power from external gratings  $P_g(t)$ , assuming an injection current of  $I/I_{th0} = 6.0$  and a phase difference of  $\psi = 0.0$ . The calculated bifurcation diagrams with the rate equations (1)–(3) are given in Figure 2. Each point in the bifurcation diagram represents a peak value of the time-varying power over the period  $t = 8 \sim 10$   $\mu$ s. The results are normalized by the time ensemble average  $\bar{P}_g$ . Figures 2(a–d) plot the bifurcation diagrams with the FG reflectivity  $R_g$  being a varied parameter when  $\alpha = 0, 2.0, 4.0,$  and  $6.0$ , respectively. In these figures, we are interested in exploring an overview of the FGSL operation over a wide range of the  $\alpha$ -factor in the limit of strong OFB. Figure 2(a) shows that the laser exhibits a CW dynamical behavior over the entire range of the strong optical feedback and when  $\alpha = 0.0$ , which means that no dynamic instability is obtained when  $\alpha$  is set to zero. By increasing the  $\alpha$ -factor

to 2.0 we get chaos, CW and periodic variation operations as shown in Figure 2(b), where the route to periodic variation or period-doubling oscillation state is CW operation, which occurs when  $R_g = 0.135$ . However, as shown in Figure 2(c) and (d), when  $\alpha = 4.0$ , and 6.0, the dynamics include CW, periodic oscillation, pulsation and chaos operations but the peak values  $P_{g(\max)}(t)$  in the chaos state is weaker associated with narrowing the chaotic region. In Figure 2(c), the transition between chaos and pulsing operations occurs through narrow range of CW operation; it is followed by wide range of CW operation and ended with weak pulsing operation (the peak values of  $P_{g(\max)}(t)$  are weak compared with first region of pulsing operation). By comparing Figure 2(d) with Figure 2(c), the transition between chaos and pulsing operations occurs through a wide range of periodic variation and ended with CW operation. The case of chaotic period-doubling operation (which induces multimode oscillation) followed by a periodic route to CW operation (as shown in Figures 2(b–d)) was also reported by Ryan et al. [18]. This means that by increasing OFB, the FGSL stability is improved at larger values of the  $\alpha$ -factor.

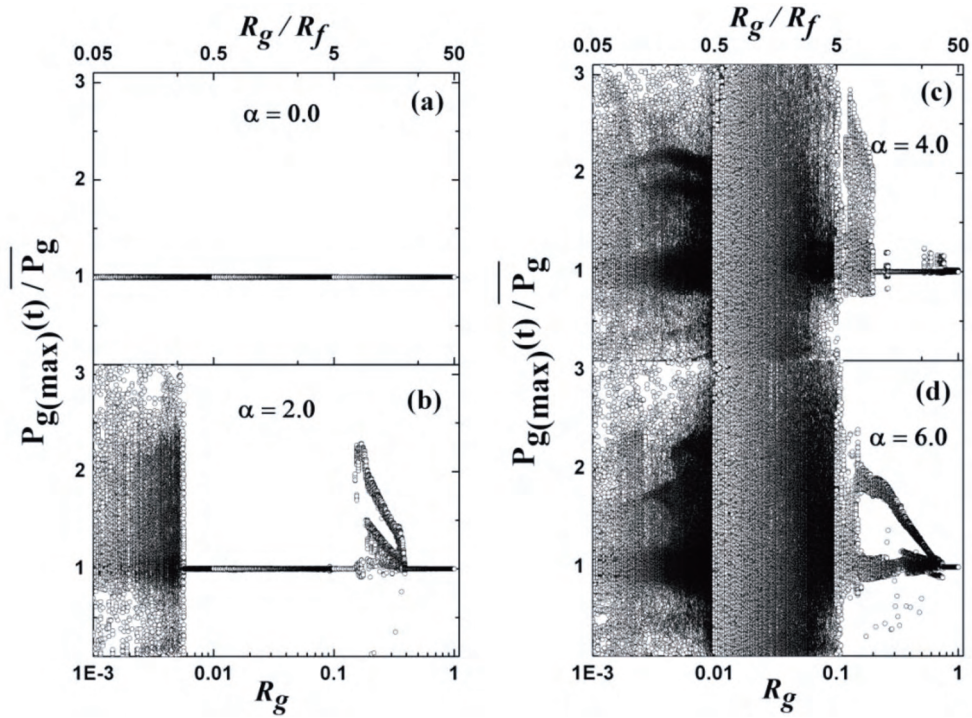


**Figure 2.** Bifurcation diagrams of a FGSL under a wide range of strong OFB and with noise sources when  $I/I_{th0} = 6.0$ : (a)  $\alpha = 0.0$ ; (b)  $\alpha = 2.0$ ; (c)  $\alpha = 4.0$ ; and (d)  $\alpha = 6.0$ . The laser mainly operates in continuous wave (CW) mode, chaos, and pulsation depending on the values of  $\alpha$ -factor and  $R_g/R_f$ .

The corresponding variation of the RIN averaged over frequencies of  $f < 10$  MHz with variation of the FG reflectivity  $R_g$  is plotted in Figure 3. As shown in Figures 3(a) and (b), the average RIN under weak OFB and when  $\alpha < 2.0$  is suppressed to the quantum noise level. The instabilities characterizing the chaotic operation under strong OFB enhance the RIN to much higher levels above the quantum level (more than 6 orders of magnitude) as shown in Figures 3(c) and (d).

The regions of pulsing operation attained under strong OFB are characterized with RIN levels of less than one order of magnitude higher than the quantum noise level.

This means that, under very strong OFB and at higher values of  $\alpha$ -parameter the output of the lasers will be more stable. The regions of moderate and higher values of  $\alpha$  factor are occupied by the operating regions of pulsation and chaos.

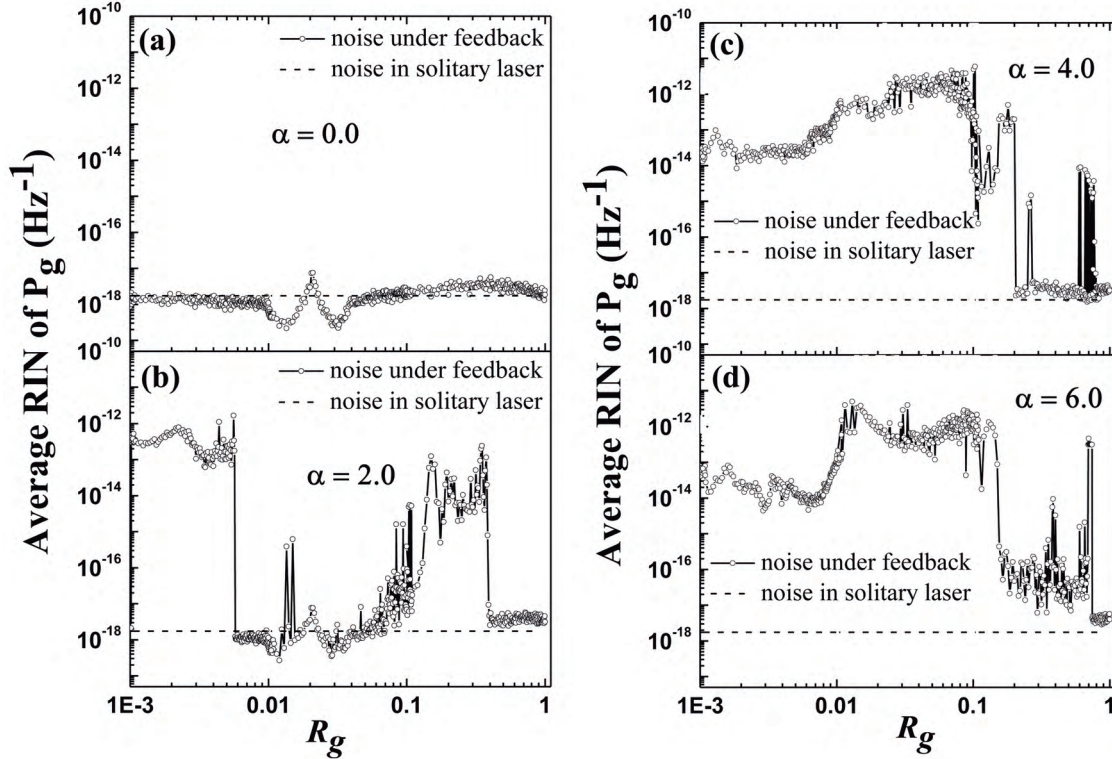


**Figure 3.** The RIN levels averaged over  $f < 10$  MHz when  $I/I_{th0} = 6.0$  : (a)  $\alpha = 0.0$ ; (b)  $\alpha = 2.0$ ; (c)  $\alpha = 4.0$ ; and (d)  $\alpha = 6.0$ .

## 4.2. Dependence on the injection current

In this section, we characterize the output power from external FG under strong OFB over a wide range of injection current:  $I = I_{th} \sim 10I_{th}$ . Figures 4(a-e) and 4(f-j) plot the bifurcation diagrams of the output power emitted from FG  $P_{g(\max)}(t)/\bar{P}$  under strong optical feedback when  $\alpha = 0, 1, 3, 5,$  and  $6$  and when the external reflectivity  $R_g = 0.07$  and  $R_g = 0.5$ , respectively. As shown in the figures, the laser operation is almost chaotic near the threshold current  $I_{th}$  at higher values of  $\alpha$  factors such as  $\alpha = 5$  and  $6$  and when  $R_g = 0.07$ . The laser operates in pulsation when it is injected well above the threshold level under very strong OFB ( $R_g = 0.5$ ) and at higher values of  $\alpha$  factor. An attractive feature of the pulsing operation is that the feedback noise is suppressed to the quantum noise level of the solitary laser when the injection current increases beyond  $7 I_{th}$ , as shown in Figures 4(i) and (j).

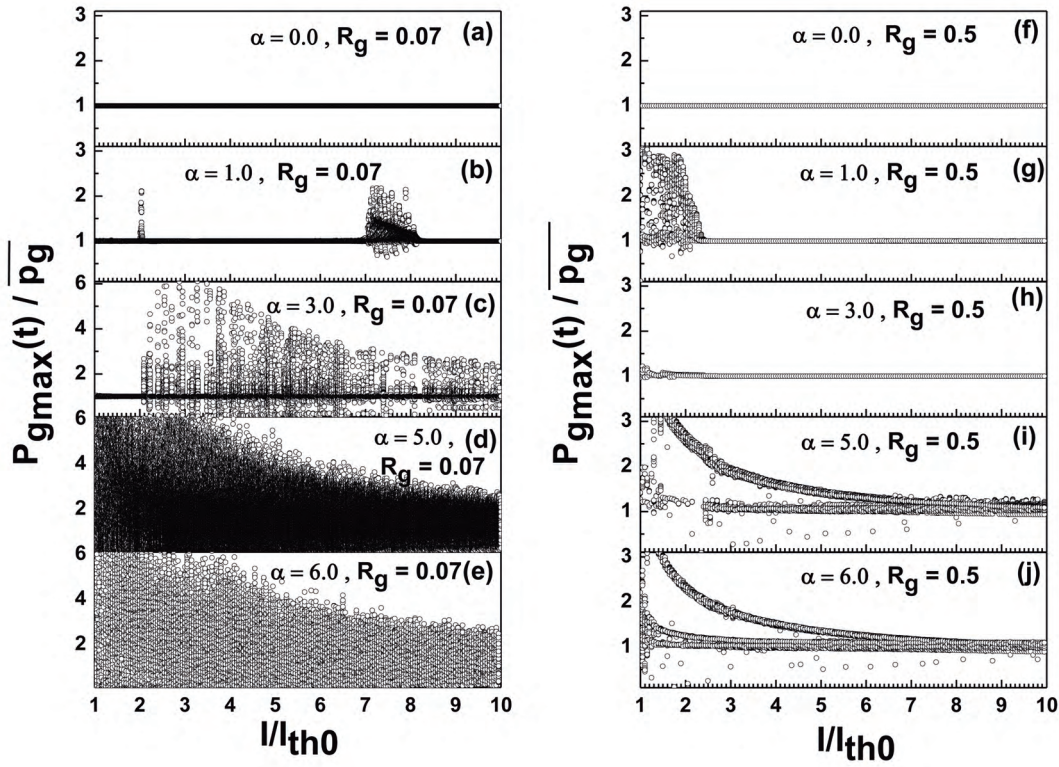


**Figure 4.** Bifurcation diagrams under strong OFB over wide range of  $I/I_{th0}$ : when  $R_g=0.07$  (a)  $\alpha = 0.0$ ; (b)  $\alpha = 1.0$ ; (c)  $\alpha = 3.0$ ; and (d)  $\alpha = 5.0$  (e)  $\alpha = 6.0$  and when  $R_g = 0.5$  (f)  $\alpha = 0.0$ ; (g)  $\alpha = 1.0$ ; (h)  $\alpha = 3.0$ ; and (i)  $\alpha = 5.0$  (j)  $\alpha = 6.0$  The laser mainly operates in CW, chaos, and pulsation depending on the values of  $\alpha$ -factor and  $R_g/R_f$  and at higher values of injection current.

### 4.3. Output power for various operating states of the FGSL

The features of the lasing operation under strong OFB can be characterized in terms of the power ratio  $P_g(t)/P_b(t)$  as shown in Figure 5, which plots the time variation of the output power ratio  $P_g(t)/P_b(t)$  for various operating states of the FGSL with noise sources. Figure 5(a) represents a typical example of the CW operation when  $\alpha = 0$  and  $R_g/R_f = 13$ . It shows that  $P_g(t)/P_b(t)$  attains a constant value with the time variation. Figure 5(b) represents pulsing variation of  $P_g(t)/P_b(t)$  when  $\alpha = 4$  and  $R_g/R_f = 13$ . The pulsing frequency in this case is  $f_{ex} = 1/\tau$ . The chaos dynamics is characterized in Figure 5(c) by random temporal variation of  $P_g(t)/P_b(t)$ . As indicated in Figure 5, the power ratio  $P_g(t)/P_b(t)$  in the pulsing operation is larger than that in the CW operation, and is more stable than that in the chaos operation. The pulsing operation in this case of strong OFB and large values of line-width enhancement factor is characterized with a low noise level that corresponds to the quantum limit. This means that the pulsing operation is more stable and is optimum for pumping optical fiber amplifiers.

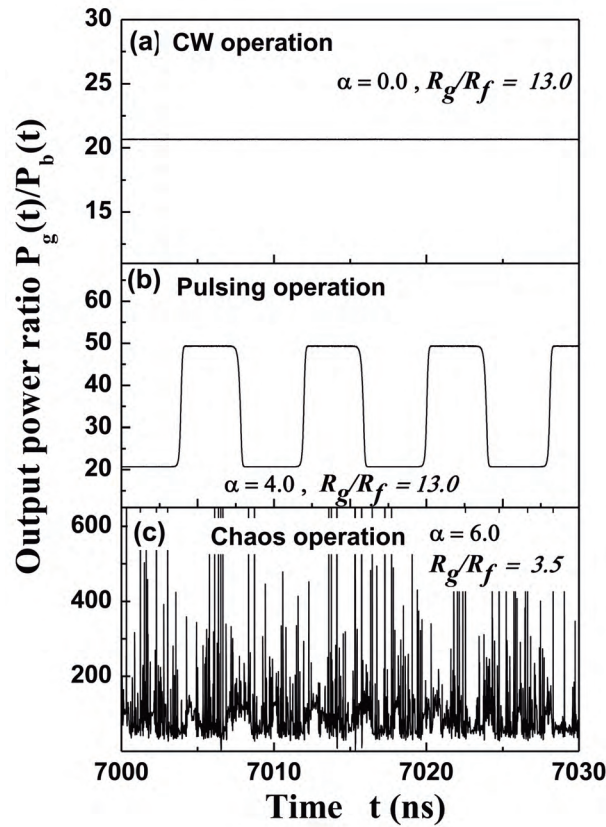


**Figure 5.** Examples of the time variation of the output power ratio  $P_g(t)/P_b(t)$  with and without noise sources under strong OFB and at several values of  $\alpha$ -factor, (a) CW, (b) pulsing and (c) chaos operations.

## 5. Conclusions

We investigated the influence of the line-width enhancement factor on the operation characteristics of FGSLs in the regime of strong OFB. The investigations were performed basing on intensive numerical integration of an improved time-delay model of semiconductor lasers. The operation characteristics were analyzed over wide ranges of strong OFB, the line-width enhancement factor and the injection current.

The operation of such FGSLs was classified as pulsing operation with small and large values of  $\alpha$ -parameter. The laser diode operates in pulsation under strong optical feedback and at small and relatively large values of the line-width enhancement factor. The associated optical feedback noise is found to be as low as the quantum noise level when the laser is operated in pulsing region and at small and relatively large values of the line-width enhancement factor. Finally, we can say that the pulsing operation of the FGSL is optimum for pumping optical fiber amplifiers because the power ratio  $P_g(t)/P_b(t)$  in the pulsing operation is larger than that in the CW operation and, on the other hand is more stable than that in the chaos operation characterized with a noise level as low as the quantum limit.

## References

- [1] G. P. Agrawal, Optical Fiber Communication Systems, (Van Nostrand Reinhold, New York. 2003), Chapter 6.
- [2] T. Mokai, K. Otsuka, *Phys. Rev.*, **55**, (1985), 1711.
- [3] A. Hohl, A. Gavrielides, *Phys. Rev. Lett.*, **82**, (1999), 1148.
- [4] Y. Kitaoka, H. Sato, K. Mizuuchi, K. Yamamoto, and M. Kato, *IEEE J. Quantum Electron.*, **32**, (1996), 822.
- [5] K. I. Kallimani and M. J. O'Mahony, *IEEE J. Quantum Electron.*, **34**, (1998), 1438.
- [6] S. Abdulrhmann, M. Ahmed, T. Okamoto and M. Yamada, 18<sup>th</sup> *IEEE Int. Semicond. Laser Conf.*, Germany, (2002), 101.
- [7] R. Lang and K. Kobayashi, *IEEE J. Quantum Electron.*, **QE-16**, (1980), 347.
- [8] S. Abdulrhmann, M. Ahmed, M. Yamada, *SPIE*, **4986**, (2003), 490.
- [9] S. Abdulrhmann, M. Ahmed, T. Okamoto, W. Ishimori, M. Yamada, *IEEE J. Select. Top. Quantum Electron.*, **9**, (2003), 1265.
- [10] S. Abdulrhmann, M. Ahmed, T. Okamoto, W. Ishimori and M. Yamada, *proceedings of The 29<sup>th</sup> Int. Sympos. Comp. Semicond.*, Lausanne, Switzerland, (2002).
- [11] S. Abdulrhmann and Minoru Yamada, *proceedings of The Second Arab International Conference in Physics and Materials Science (CPMS)*, Alexandria, Egypt, October, (2007), 27.
- [12] S. Abdulrhmann, *proceedings of The Sixth International Conference on wireless and Optical communications Networks (WOCN2009)*, Cairo Egypt, April 28 - 30, (2009).
- [13] S. Abdulrhmann, M. Yamada and M Ahmed, *International Journal of Numerical Modelling: Electronic Networks, Devices and Fields*, **24**, (2011), 218.
- [14] C. H. Henry, *IEEE J. Quantum Electron.*, **QE-18**, (1982), 259.
- [15] M. Osinski and J. Buss, *IEEE Journal Quantum Electron*, **23**, (1987), 9.
- [16] C. Masoller and N. B. Abraham, *Phys. Rev. A*, **57**, (1998), 1313.
- [17] D. Rodriguez, I. Esquivias, S. Deubert, J. P. Reithmaier, A. Forchel, M. Krarowski, M. Calligaro, and O. Parillaud, *IEEE J. Quantum Electron.*, **41**, (2005), 117.
- [18] A. T. Ryan, G. P. Agrawal, G. R. Gray, and E. C. Gage, *IEEE J. Quantum Electron.*, **30**, (1994), 668.
- [19] Z. Mi, P. Bhattacharya, and S. Fathpour, *Appl. Phys. Lett.*, **86**, (2005), 153109.
- [20] Z. Mi and P. Bhattacharya, *IEEE J. Quantum Electron.*, **43**, (2007), 363.
- [21] M. Ahmed, M. Yamada and S. Abdulrhmann, *AIUB*, **7**, (2008), 1.
- [22] M. Ahmed and M. Yamada, *IEEE J. Quantum Electron.*, **38**, (2002), 682.
- [23] M. Ahmed and M. Yamada, *J. Appl. Phys.*, **84** (1998), 3004
- [24] S. Melnik and G. Huyet, *OPTICS EXPRESS*, **14**, (2006), 2950.
- [25] Z. Mi and P. Bhattacharya, *IEEE J. Quantum Electron.*, **43**, (2007), 363.